

The Influence of the Gear Reduction Ratio on the Free-floating Space Manipulator's Dynamics

Mateusz Wojtunik^a and Karol Seweryn^b

Centrum Badań Kosmicznych Polskiej Akademii Nauk (CBK PAN), Warsaw, Poland

Keywords: Space Robotics, Free-floating Manipulators, Gear-equipped Space Manipulators, Gear Reduction Ratio.

Abstract: Utilisation of space manipulator mounted on the satellite is one of the main methods for the proposed Active Debris Removal and On-Orbit Servicing missions. Precise numerical models of the manipulator's joint are very important as its dynamics has a strong effect on the behaviour of the system including the base where it is mounted. One of aspects that can be considered is the extension of manipulator's dynamical equations with gear kinematic constraints. To achieve this goal, dynamical equations of motion for planar 3DoF free-floating manipulator with gear kinematic constraints are presented in this paper. Open-loop analysis is performed to form conclusions concerning the influence of the gear reduction ratio on space manipulator's dynamics. Torques required to perform end-effector straight line trajectory are evaluated using inverse dynamics path planning algorithm and then utilised as motor driving torques for different gear reduction ratios. It appears that the gear reduction ratio influences the system mass matrix nonlinearly causing the end-effector trajectory to deviate from the straight line. These deviations are already observed for relatively low gear reduction ratios.


1 INTRODUCTION


Orbital robotics is becoming the field of research in demand for the case of future Active Debris Removal (ADR) technologies and On-Orbit Servicing (OOS) missions (NASA, 2010). Increasing number of space debris poses an important issue as collisions probability ascends. It is projected that removing space debris will help to maintain the number of space objects at relatively constant value (Liou, 2011). In addition, studies suggest that ADR and OOS missions will be economically feasible (Sullivan and Akin, 2012). European Space Agency stated that one of its main four goals is to widen contribution of European consortia in space debris removal development before 2030 (ESA, 2019).

Space manipulators will have a significant role in terms of ADR technologies development. Space debris are most commonly noncooperative, thus unmanned autonomous systems are needed to perform the capture manoeuvre. There has already been a lot of research done considering utilisation of space manipulator for ADR. One of them is the e.Deorbit mission designed to capture Envisat

satellite (Estable et al., 2020). Another mission that is worth mentioning is DARPA's Orbital Express (Ogilvie, Allport, Hannah and Lymer, 2008). This project led to successful demonstration of capture manoeuvre of NEXTSat satellite using 6DoF robotic arm.

Utilisation of free-floating manipulators poses a lot of advantages in terms of designing ADR or OOS missions. One of them is their high Technology Readiness Level (TRL). Moreover, they are relatively easy to be tested on ground in comparison to e.g. net capturing (Shan, Guo and Gill, 2016). However, space manipulators require designing complex control algorithms taking extreme work environment into the consideration (Siciliano and Khatib, 2008). First challenge appears as space manipulators are characterised with free-floating base that moves via reaction forces and torques induced by manipulator's motion. Free-floating base is widely considered in terms of path planning algorithms. Numerous trajectory planning methods are presented in literature, e.g. considering nonlinear optimisation (Lampariello, 2010), control torque minimisation (Rybus, Seweryn and Szaśiadek, 2016) or obstacles

^a  <https://orcid.org/0000-0002-0234-2368>

^b  <https://orcid.org/0000-0002-4372-0900>

avoidance (Rybus and Seweryn, 2015). In addition, capture manoeuvre analysis has to concern contact dynamics between the gripper and the client satellite (Korf, 1982).

Finally, joint dynamics have a much stronger effect on the system behaviour than it is observed for manipulators working on the Earth. This poses the need for designing precise numerical models of the joint. One of the most popular aspects considered in mathematical models is joint flexibility. This is extremely important as it induces additional eigenfrequencies of the system causing the end-effector to oscillate or lose stability (Sąsiadek, 2013). Flexible-joint manipulator models are widely described with different model configurations. Fixed-base assumption is considered by Ulrich and Sąsiadek (2012). Analysis for the maximum load of flexible-joint manipulators is performed by Korayem, A., Irani, Babae and Korayem, M. (2017). Free-floating base is introduced e.g. by Yu (2015). In addition, wheeled mobile manipulators are also analysed (Korayem and Ghariblu, 2003). Moreover, flexible links are often considered (Korayem, Rahimi and Nikoobin, 2011). The analysis is also extended with joint friction (Qingxuan, 2008), (Liu, Li, Wang and Cai, 2015). The generalised mathematical model for the free-floating flexible-joint manipulator is described by Nanos and Papadopoulos (2015).

Another important aspects are both dynamics and kinematics of manipulator gears. Despite the fact that including the gear kinematic constraint for space manipulators is not widely considered in the literature, it is often introduced in the flexibility models e.g. (Qingxuan, 2008) and (Nanos and Papadopoulos, 2015). However, there is no straightforward analysis of the influence of the gear on the dynamics of the free-floating manipulator. In this paper we provide an explanation for modifications arising from extending space manipulator's mathematical model with gear constraints. This also shows the importance of the common model assumption that driving torques are applied in manipulator's joints directly to its links. Consideration of additional effects could pose conclusions for the choice of the control algorithm. In addition, including precise numerical model of the joint in the control algorithm may be beneficial for the control quality.

In this paper we present dynamical equations for the gear-equipped planar 3DoF space manipulator with control torques applied to motors. Open-loop analysis is performed to pose conclusions for the influence of the gear reduction ratio on the dynamical behaviour of the system. The paper is organised as

follows. Dynamical equations of the analysed system are presented in Section 2, whereas the simulation results are described in Section 3. Section 4 concludes the paper with a summary.

2 DYNAMICAL EQUATIONS

In this section, equations for the planar 3DoF free-floating space manipulator are introduced as well as the extension of the gear kinematic constraint is presented. The model is based on equations presented by Rybus et al. (2016) and originated from the algorithm introduced by Seweryn and Banaszkiwicz (2008).

2.1 Planar 3DoF Free-floating Space Manipulator

Coordinate systems and state variables are defined on the schematic view and shown in Figure 1. Generalised coordinates vector of the system \mathbf{q} includes base X and Y position components and its orientation as well as manipulator's joint angles:

$$\mathbf{q} = [x_0 \quad y_0 \quad q_0 \quad q_1 \quad q_2 \quad q_3]^T \quad (1)$$

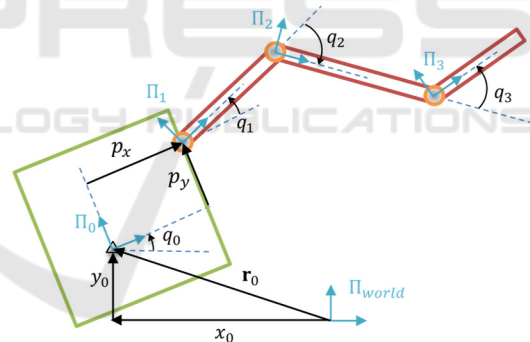


Figure 1: Schematic view of the planar 3DoF satellite-manipulator system.

We follow the Lagrange formalism to achieve the set of dynamical equations of the system (Schaub and Junkins, 2002). The generalised forces vector \mathbf{Q} for the analysed system is given by:

$$\mathbf{Q} = [F_x \quad F_y \quad \tau_0 \quad \tau_1 \quad \tau_2 \quad \tau_3]^T \quad (2)$$

where F_x and F_y denote X and Y components of the force acting on the base centre of mass, respectively, τ_0 denotes torque acting on the base centre of mass, whereas τ_1 , τ_2 and τ_3 are joint torques.

When the satellite-manipulator system is in the proximity of the client satellite, base control system is considered to be turned off, therefore the first three

components of \mathbf{Q} are equal to zero. The consequence of this assumption is that the system has conserved total momentum and angular momentum – joint driving torques are of internal nature. Moreover, it is widely assumed that the space manipulator does not have potential energy as gravity forces are negligible, thus Lagrange function becomes the total kinetic energy of the system calculated as:

$$E_k = \frac{1}{2}m_0(\dot{x}_0^2 + \dot{y}_0^2) + \frac{1}{2}I_0\dot{q}_0^2 + \frac{1}{2}\sum_{i=1}^3 m_i \mathbf{v}_i^T \mathbf{v}_i + \frac{1}{2}\sum_{i=1}^3 I_i \omega_i^2 \quad (3)$$

where \dot{x}_0 and \dot{y}_0 denotes components of the linear velocity of the satellite centre of mass, \dot{q}_0 denotes the angular velocity of the satellite, m_0 denotes the mass of the satellite and I_0 is the inertia of the satellite, m_i denotes the mass of the i -th link and I_i is the inertia of the i -th link, whereas \mathbf{v}_i denotes the i -th link centre of mass translational velocity vector and ω_i is the i -th link angular velocity in Π_{world} frame evaluated as:

$$\omega_i = \dot{q}_0 + \sum_{j=1}^i \dot{q}_j \quad (4)$$

where \dot{q}_j denotes the angular velocity of j -th joint with respect to the previous joint Π_{i-1} .

The translational velocity vector of each link centre of mass is derived from differentiating its position components arising from kinematical equations of the satellite-manipulator system. After such derivation, the total kinetic energy of the system (3) becomes dependent upon generalised coordinates and velocities of the system. Thus, it can be differentiated to expand the Euler-Lagrange equations. This leads to the final formula for dynamical equations of the free-floating manipulator that can be expressed in the following form:

$$\mathbf{M}(\mathbf{q})\ddot{\mathbf{q}} + \mathbf{C}(\mathbf{q}, \dot{\mathbf{q}})\dot{\mathbf{q}} = \mathbf{Q} \quad (5)$$

where $\mathbf{M}(\mathbf{q})$ denotes a [6x6] system mass matrix that satisfies the following relation:

$$E_k = \frac{1}{2}\dot{\mathbf{q}}^T \mathbf{M}(\mathbf{q})\dot{\mathbf{q}} \quad (6)$$

In (5) $\mathbf{C}(\mathbf{q}, \dot{\mathbf{q}})$ denotes a [6x6] centrifugal and Coriolis forces matrix defined as:

$$\mathbf{C}(\mathbf{q}, \dot{\mathbf{q}}) = \left(\dot{\mathbf{M}}(\mathbf{q}, \dot{\mathbf{q}}) - \frac{1}{2} \frac{\partial}{\partial \mathbf{q}} [\mathbf{M}(\mathbf{q})\dot{\mathbf{q}}] \right)^T \quad (7)$$

where $\dot{\mathbf{M}}(\mathbf{q}, \dot{\mathbf{q}})$ denotes the time derivative of the mass matrix.

Analytical equations posing each element of $\mathbf{M}(\mathbf{q})$ and $\mathbf{C}(\mathbf{q}, \dot{\mathbf{q}})$ are presented in (Wojtunik, 2020).

Derived relations allow to define dependencies of joints driving torques for the given satellite-manipulator system trajectory defined in the generalised coordinates. Equation (5) can be finally solved for $\ddot{\mathbf{q}}$ to form a set of differential equations of the system:

$$\ddot{\mathbf{q}} = \mathbf{M}^{-1}(\mathbf{q})[\mathbf{Q} - \mathbf{C}(\mathbf{q}, \dot{\mathbf{q}})\dot{\mathbf{q}}] \quad (8)$$

2.2 Gear Kinematic Constraint

Set of equations derived in the previous section assumed that manipulator joints are the ideal source of driving torques. However, there are many modelling aspects that can extend the model. One of them is the kinematic constraint of the gear. In this section the approach for modelling gear kinematics is presented.

In order to introduce the gear kinematic constraint, the additional body – motor – must be considered to be rotating in each joint. The schematic view of the joint equipped with gear is depicted in Figure 2. i -th motor and i -th link are considered to be rotating around the same axis. In contrast to discussion in the previous section, the driving torque will now be applied to the motor instead of being directly applied to the link.

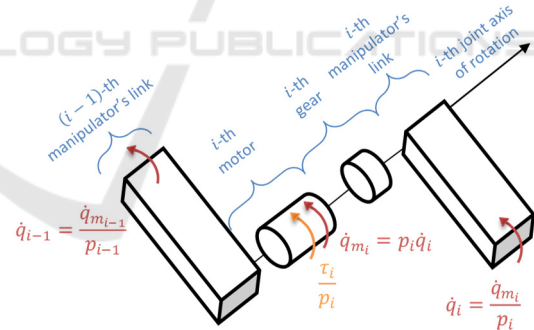


Figure 2: Schematic view of manipulator joint equipped with gear.

Motors and links are connected via gear which leads to the following kinematic constraint:

$$\dot{q}_{m_i} = p_i \dot{q}_i \quad (9)$$

where \dot{q}_{m_i} denotes motor angular velocity with respect to the previous joint Π_{i-1} (similarly to \dot{q}_i) and p_i denotes i -th gear reduction ratio taking values greater or equal to 1.

The following approach of deriving set of equations for the free-floating manipulator equipped with gears will take advantage of relations posed in

the previous section. Total kinetic energy of the system (3) must be expanded with total motors' kinetic energy defined below. It is assumed that motor mass is included in the link mass, therefore only rotational kinetic energy is considered:

$$E_{k_m} = \sum_{i=1}^3 I_{m_i} \omega_{m_i}^2 \quad (10)$$

where I_{m_i} denotes the inertia of the i -th motor and ω_{m_i} denotes the i -th motor angular velocity in Π_{world} frame defined as:

$$\omega_{m_i} = \begin{cases} \dot{q}_0 + \dot{q}_{m_i}, & i = 1 \\ \dot{q}_0 + \sum_{j=1}^{i-1} \dot{q}_j + \dot{q}_{m_i}, & i > 1 \end{cases} \quad (11)$$

Algebraic constraint (9) allows us to decrease the system order by posing \dot{q}_{m_i} as a function of \dot{q}_i or vice versa. It is more intuitive to choose motor variables as the generalised coordinates because driving torques are no longer applied to links. Thus, the generalised coordinates vector becomes:

$$\mathbf{q}_g = [x_0 \quad y_0 \quad q_0 \quad q_{m_1} \quad q_{m_2} \quad q_{m_3}]^T \quad (12)$$

Equations (3) and (10) form the total kinetic energy of the system dependent upon \mathbf{q}_g and $\dot{\mathbf{q}}_g$ that is substituted to the Euler-Lagrange equation. Similarly to the approach presented in section 2.1, required derivatives are calculated to form a final set of dynamical equations of the system:

$$\mathbf{M}_g(\mathbf{q}_g) \ddot{\mathbf{q}}_g + \mathbf{C}_g(\mathbf{q}_g, \dot{\mathbf{q}}_g) \dot{\mathbf{q}}_g = \mathbf{Q}_g \quad (13)$$

where \mathbf{Q}_g is the generalised forces vector containing motor driving torques scaled using gear reduction ratios:

$$\mathbf{Q}_g = \left[F_x \quad F_y \quad \tau_0 \quad \frac{\tau_1}{p_1} \quad \frac{\tau_2}{p_2} \quad \frac{\tau_3}{p_3} \right]^T \quad (14)$$

Finally, equation (13) is solved for $\ddot{\mathbf{q}}_g$:

$$\ddot{\mathbf{q}}_g = \mathbf{M}_g^{-1}(\mathbf{q}_g) [\mathbf{Q}_g + \mathbf{C}_g(\mathbf{q}_g, \dot{\mathbf{q}}_g) \dot{\mathbf{q}}_g] \quad (15)$$

Analytical relations for $\mathbf{M}_g(\mathbf{q}_g)$ and $\mathbf{C}_g(\mathbf{q}_g, \dot{\mathbf{q}}_g)$ are too complex to be presented. Instead, a brief description of deviations between obtained models is provided below. The mass matrix as well as the Coriolis matrix of the satellite-manipulator system equipped with gears differ from matrices depicted in (5). As a result of introducing gear constraint (9) inertia components of links will now be scaled by gear reduction ratios p_i . i -th link inertia and mass components located within the main diagonal of

$\mathbf{M}_g(\mathbf{q}_g)$ are scaled by p_i^2 , whereas outside the main diagonal they are scaled by p_i . In addition, as multiple-joint manipulator is considered, some components of the mass matrix can be scaled by the multiplication of different gear reduction ratios. Similarly, some components of $\mathbf{C}_g(\mathbf{q}_g, \dot{\mathbf{q}}_g)$ are dependent upon gear reduction ratios. The above-mentioned observations pose neuralgic nonlinear influence of p_i on the dynamics of the system which will be analysed in the next section.

3 NUMERICAL SIMULATIONS

The influence of the gear reduction ratio on the dynamics of the free-floating space manipulator will be analysed in this section. The discussion will concern the open-loop analysis for the straight line trajectory of the manipulator's end-effector.

In order to find required driving torques for the given end-effector trajectory, we follow the inverse dynamics approach for path planning introduced by Basmadji, Seweryn and Saşiadek (2020). First of all, required generalised coordinates, velocities and accelerations to achieve end-effector straight line trajectory are calculated for the given initial satellite-manipulator system's state. The initial momentum and angular momentum of the system is set to be zero. Manipulator's parameters are set to reflect the prototype built in the Space Research Centre of the Polish Academy of Sciences (Basmadji, Chmaj, Rybus and Seweryn, 2019) and are shown in Table 1. The end-effector is chosen to travel 0.4 m along the X axis (from 1.5 m to 1.1 m), maintaining constant Y position (0 m) and orientation ($\frac{\pi}{6}$ rad) expressed in Π_{world} . Then, equation (5) is used to evaluate the desired driving torques required to achieve the planned trajectory. The trajectory (red line) of the manipulator is shown in Figure 3. Computed driving torques in each joint are presented in Figure 4.

Driving torques required to perform straight line trajectory are then scaled with gear reduction ratios (14) and used to actuate the manipulator model with gears (15). Numerical model of the satellite-manipulator system is designed in Matlab/Simulink with the use of Simscape SimMechanics library. This model poses the system of identical mathematical description as in (15). The model is solved with IV order Runge-Kutta method (ode4). The integration time step is set to 0.01 s.

It is important for the gear-equipped manipulator model to maintain the same total inertia of the system as the reference model. Thus, if nonzero motor inertia

is introduced, respective link inertia has to be decreased in a specific manner. For following simulations, each motor inertia is set to 10^{-5} kgm^2 . In addition, it is assumed that gear reduction ratios in all joints are equal.

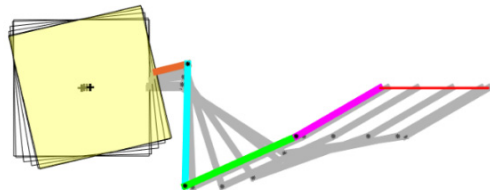


Figure 3: Analysed end-effector trajectory.

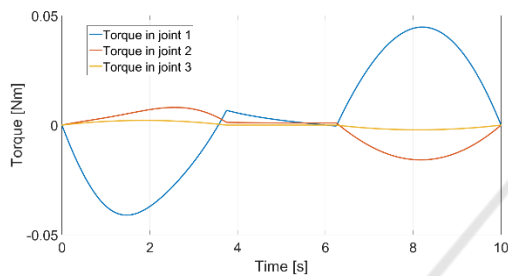


Figure 4: Computed driving torques.

Table 1: Satellite-manipulator system parameters.

Parameter	Value
Satellite mass	64.859 kg
Satellite inertia	2.695 kgm^2
Manipulator mounting point	[0.370, 0.001] m
Link 1 mass	2.913 kg
Link 1 inertia	0.091 kgm^2
Link 1 length	0.449 m
Link 1 centre of mass position	[0.181, 0] m
Link 2 mass	2.646 kg
Link 2 inertia	0.081 kgm^2
Link 2 length	0.450 m
Link 2 centre of mass position	[0.200, 0] m
Link 3 mass	1.699 kg
Link 3 inertia	0.022 kgm^2
Link 3 length	0.355 m
Link 3 centre of mass position	[0.103, -0.002] m

The following values of gear reduction ratio are analysed: 1, 1.05, 1.1, 1.25, 1.5, 2.5, 5 and 10. End-effector trajectories for each simulation are compared in Figure 5. Final configurations for the manipulator (excluding $p = 1$) are presented in Figure 6. Manipulator's joint velocities are presented in Figure 7. Base position components and orientation are shown in Figure 8. In addition, end-effector's position errors in the final configuration are presented in Table

2, where X and Y errors are derived as the difference between the respective position components in comparison to the reference case. The error norm is calculated as the square-root of the sum of squares of the above-mentioned errors.

It is observed that if the gear reduction ratio is equal to one then the model acts numerically identical to the reference case – mass matrices for both models are indistinguishable.

The analysis shows that the straight line trajectory is not projected well even for relatively low gear reduction ratios – the error norm surpasses 5 cm already for $p = 1.25$. The Y component error for $p = 10$ reaches over 25 cm whereas the X component error exceeds 10 cm. These errors are observed because manipulator joint trajectories are not equal to desired ones that result from the reference model. Another consequence is observed in Figure 8 where satellite position and orientation deviations are seen. The reason behind these results is related to gear reduction ratio's appearance in the mass matrix of the system. As stated in the previous section, this parameter scales the matrix nonlinearly – some inertia components are scaled with p^2 , others with p and there is also a group of components that are not scaled at all. The nonlinear nature of this influence is well observed in Figure 6 where e.g. deviations between simulations with $p = 10$ and $p = 5$ have different magnitude than differences between simulations with $p = 2$ and $p = 1$. It appears that torque signals that have to be applied to motors in order to provide straight line trajectory have different shape than those calculated for the reference model. In addition, the above-mentioned scaling is quite extreme, as e.g. $p = 5$ can decrease link inertia seen by the motor even 25 times. If we were to provide that links' velocities are exactly the same as it appears for the planned trajectory, the end-effector would project the straight-line independently of p , because it is assumed that the overall inertia of the joint is identical for both

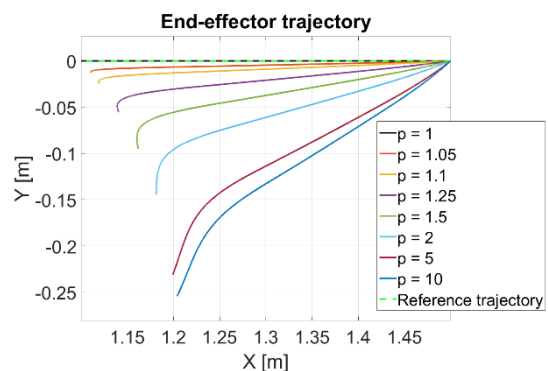


Figure 5: Comparison of end-effector trajectories for simulations with different gear reduction ratios.

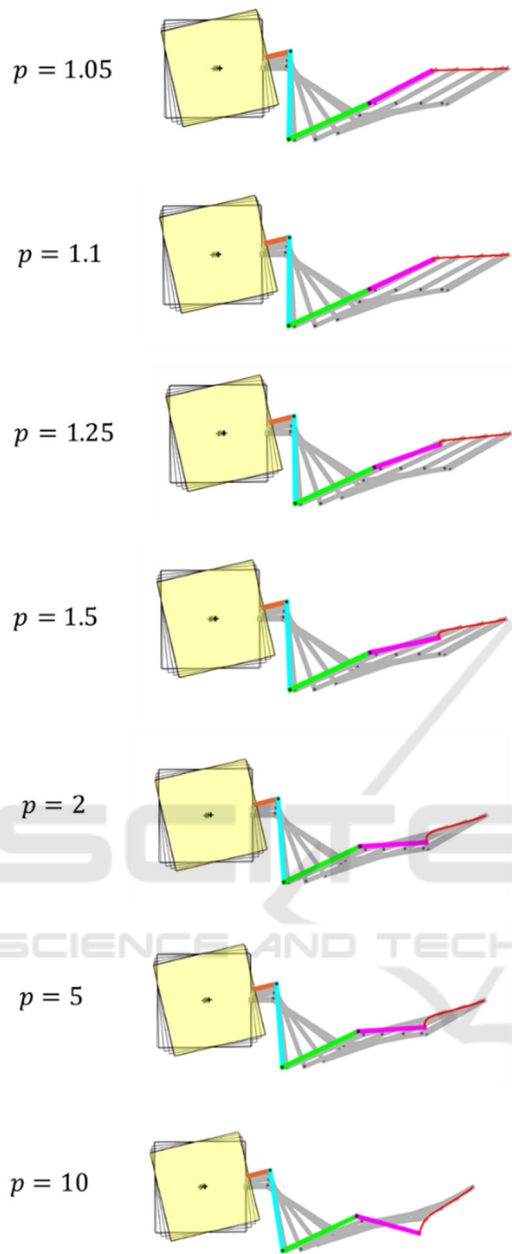


Figure 6: End-effector trajectories for simulations with different gear reduction ratios.

reference and extended model. However, achieving the same joint velocities require different torque signals as equation (13) differs from (5). This leads to a conclusion that in the closed-loop case based on equation (5) control signals from space manipulator controller are obliged to compensate errors induced by the gear influence on the dynamics of the system. These observations pose an important issue that arises from the assumption of applying driving torques directly to manipulator's links. It appears that this

Table 2: End-effector position errors in the final configuration for different gear reduction ratios.

Gear reduction ratio	X position error [m]	Y position error [m]	Error norm [m]
1.05	0.0105	-0.0127	0.0165
1.1	0.0196	-0.0246	0.0314
1.25	0.0404	-0.0555	0.0686
1.5	0.0615	-0.0947	0.1129
2	0.0810	-0.1447	0.1658
5	0.0991	-0.2309	0.2513
10	0.1037	-0.2544	0.2748

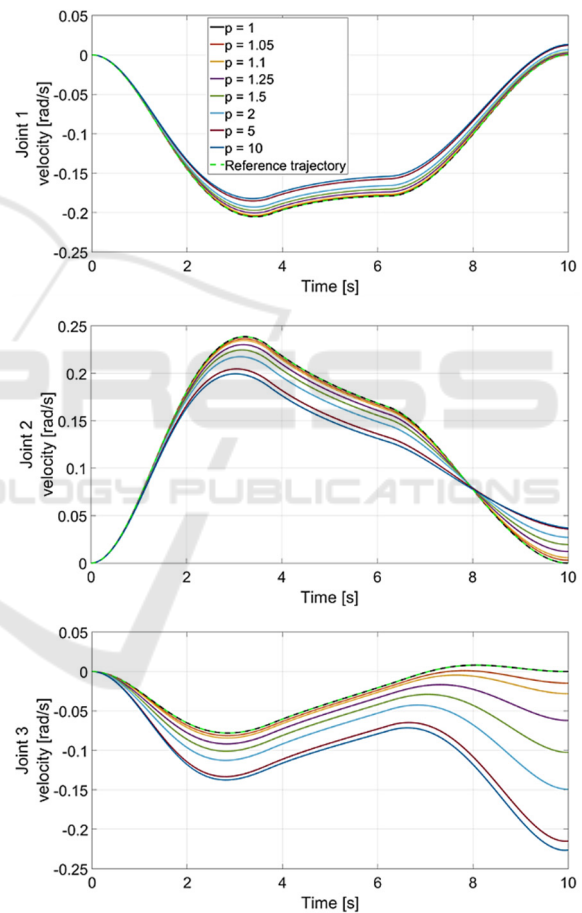


Figure 7: Joint velocities for simulations with different gear reduction ratios.

supposition causes driving torques to differ from signals that could be required to perform specific task by the satellite-manipulator system designed for space mission. Therefore, it is concluded that precise joint models can provide greater verifiability of the simulation tool as it magnifies dynamical behaviour

caused by gears. It can also be beneficial to include such aspects in the control system.

In addition, it is interesting to observe the final manipulator's configurations seen in Figure 5. For instance, for the highest analysed gear reduction ratio the third link has much more deviated position than it is seen for other simulation cases. The nonzero third joint velocity at the end of the simulation (Figure 7) causes the end-effector trajectory to deviate towards negative Y positions.

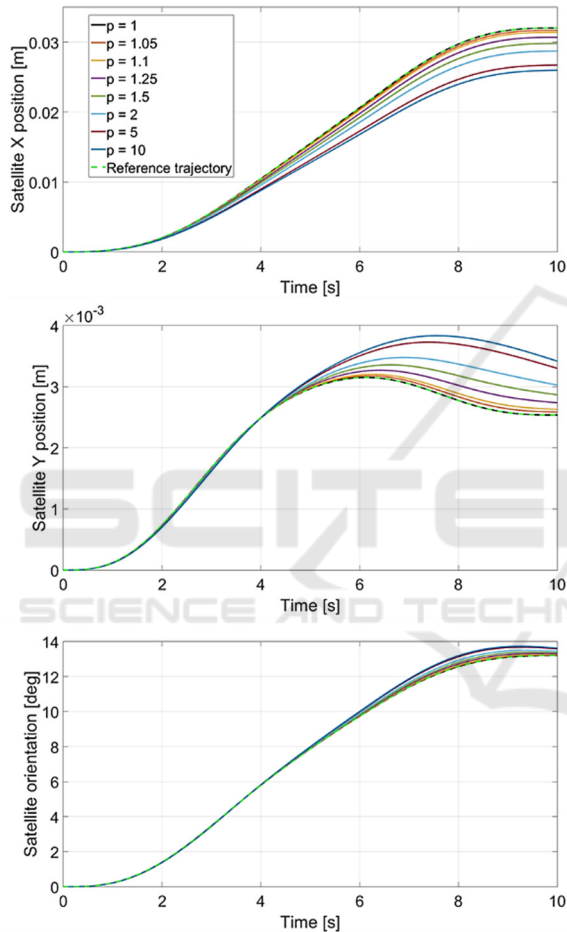


Figure 8: Satellite position and orientation for simulations with different gear reduction ratios.

4 CONCLUSIONS

The modified free-floating satellite-manipulator system model with the kinematic gear constraints allowed to pose conclusions regarding the influence of the gear reduction ratio on the dynamics of the system. Lagrange functions for both reference and newly discussed model were used to derive dynamical equations of the system and observe

differences in the system mass matrix components induced by the constraint. It appears that both mass matrix and Coriolis and centrifugal forces matrix are dependent nonlinearly upon the gear reduction ratio. The influence of this parameter on the dynamics of the system was analysed by applying reference driving torque signals to actuate the extended model. It turned out that the planned straight line trajectory is not projected well by the model concerning joint gears. It presents the importance of modelling gear kinematic constraints as the control system will be working under different circumstances than it is posed by the reference model. Designing a precise model of space manipulator's joint is therefore extremely important to provide greater verifiability of the simulation tool. The future work may include analysis of motor driving torques in the closed-loop system for the manipulator equipped with gears. In addition, the derived model could be extended with additional aspects such as joints' or links' flexibility, joint friction or dynamics of the gear.

ACKNOWLEDGEMENTS

This paper was partially supported by the Polish National Centre for Research and Development in the frame of the LIDER X programme (project no. LIDER/19/0117/L-10/18/NCBR/2019).

The Author would like to thank Dr. Tomasz Rybus from the Space Mechatronics and Robotics Laboratory at Centrum Badań Kosmicznych Polskiej Akademii Nauk (CBK PAN) for his helpful suggestions.

REFERENCES

- Basmadji, F. L., Chmaj, G., Rybus, T. and Seweryn, K. (2019). *Microgravity testbed for the development of space robot control systems and the demonstration of orbital maneuvers*. Photonics Applications in Astronomy, Communications, Industry, and High-Energy Physics Experiments, Wilga, Poland.
- Basmadji, F. L., Seweryn, K. and Sasiadek, J. Z. (2020). Space robot motion planning in the presence of linear and angular momenta. *Multibody System Dynamics* (vol. 50, pp. 71-96).
- ESA's *Technology Strategy* (2019). European Space Agency, v1.1.
- Estable, S., Pruvost, C., Ferreira, E., Telaar, J., Frunhert, M., Imhof, C., Rybus, T., et al. (2020). Capturing and deorbiting Envisat with an Airbus Spacetug. Results from the ESA e.Deorbit consolidation phase study. *Journal of Space Safety Engineering* (vol. 7, pp. 52-66).

- Korayem, A. H., Irani, M., Babae, H. and Korayem, M. H. (2017). Maximum load of flexible joint manipulators using nonlinear controllers. *Robotica* (vol. 35, no. 1, pp. 119-142).
- Korayem, M. H., Rahimi, A. and Nikoobin, A. (2011). Path Planning of Mobile Elastic Robotic Arms by Indirect Approach of Optimal Control. *Journal of Advanced Robotic Systems* (vol. 8, no. 1, pp. 10-20).
- Korayem, M. H. and Gariblu, H. (2003). Maximum Allowable Load on Wheeled Mobile Manipulators Imposing Redundancy Constrains. *Robotics and Autonomous Systems* (no. 44, pp. 151-159).
- Korf, R. E. (1982). *Space robotics*. Carnegie-Mellon University, The Robotics Institute.
- Lampariello, R. (2010). *Motion Planning for the On-orbit Grasping of a Non-cooperative Target Satellite with Collision Avoidance*. 10th International symposium on Artificial Intelligence, Robotics and Automation In Space, Sapporo, Japan.
- Liou, J. C. (2011). An active debris removal parametric study for LEO environment remediation. *Advances in Space Research* (vol. 47(11), pp. 1865-1876).
- Liu, X., Li, H., Wang, J. and Cai, G. (2015). Dynamics analysis of flexible space robot with joint friction. *Aerospace Science and Technology* (vol. 47, pp. 164-176).
- Nanos, K. and Papadopoulos, G. (2015). On the dynamics and control of flexible joint space manipulator. *Control Engineering Practise* (vol. 45, pp. 230-143).
- Ogilvie, A., Allport, J., Hannah, M. and Lymer, J. (2008). *Autonomous satellite servicing using the Orbital Express Demonstration Manipulator System*. 9th International Symposium on Artificial Intelligence, Robotics and Automation in Space, Hollywood, USA.
- On-orbit Satellite Servicing Study* (2010). NASA, Technical Report.
- Qingxuan, J., Xiaodong, Z., Hanxu, S. and Ming, C. (2008). *Active Control of Space Flexible-Joint/Flexible-Link Manipulator*. IEEE Conference on Robotics, Automation and Mechatronics, Chengdu, China.
- Rybus, T. and Seweryn, K. (2015). *Application of Rapidly-exploring Random Trees (RRT) algorithm for trajectory planning of free-floating space manipulator*. Proceedings of the 10th International Workshop on Robot Motion and Control, Poznan, Poland.
- Rybus T., Seweryn K. and Sasiadek, J. Z. (2016). *Trajectory Optimization of Space Manipulator with Non-zero Angular Momentum During Orbital Capture Maneuver*. AIAA Guidance, Navigation and Control Conference, San Diego, USA.
- Sasiadek, J. Z. (2013). Space Robotics and its Challenges. *Aerospace Robotics*. GeoPlanet: Earth and Planetary Sciences, Springer (pp. 1-8).
- Schaub, H. and Junkins, J. L. (2002). *Analytical Mechanics of Aerospace Systems*. American Institute of Aeronautics and Astronautics, Inc.
- Seweryn, K. and Banaszkiwicz, M. (2008). *Optimization of the trajectory of a general free-flying manipulator during the rendezvous maneuver*. Proceedings of the AIAA Guidance, Navigation, and Control Conference and Exhibit (AIAA-GNC'2008), Honolulu, USA.
- Shan, M., Guo, J. and Gill, E. (2016). Review and comparison of active space debris capturing and removal. *Progress in Aerospace Sciences* (vol. 80, pp. 18-32).
- Siciliano, B. and Khatib, O. (2008). *Springer Handbook of Robotics*, Springer.
- Sullivan, B. and Akin, D. (2012). *Satellite servicing opportunities in geosynchronous orbit*. Proceedings of the AIAA SPACE 2012 Conference and Exposition, Pasadena, USA.
- Ulrich, S. and Sasiadek, J. Z. (2012). Modelling and Direct Adaptive Control of a Flexible-Joint Manipulator. *Journal of Guidance, Control, and Dynamics* (vol. 35(1), pp. 25-39).
- Wojtunik, M. (2020). *Modelling and validation of space robot's joint*. Master's thesis (in Polish: Opracowanie i walidacja modelu matematycznego złącza manipulatora satelitarnego), Technical University of Lodz.
- Yu, X.-Y. (2015). Augmented robust control of a free-floating flexible space robot. *Journal of Aerospace Engineering* (vol. 229(5), pp. 947-957).